ACS PHYSICAL CHEMISTRY Au
AN OPEN ACCESS JOURNAL OF THE AMERICAN CHEMICAL SOCIETY

pubs.acs.org/physchemau
Article

Isomeric Identification of the Nitroindole Chromophore in Indole + NO_3 Organic Aerosol

Avery B. Dalton, Lisa M. Wingen, and Sergey A. Nizkorodov*

Cite This: ACS Phys. Chem Au 2024, 4, 568−574
Read Online

ACCESS | Metrics & More | Article Recommendations | Supporting Information

ABSTRACT: Oxidation of indole by nitrate radical (NO_3) was previously proposed to form nitroindole, largely responsible for the brown color of indole secondary organic aerosol (SOA). As there are seven known nitroindole isomers, we used chromatographic separation to show that a single nitroindole isomer is produced in the indole + NO_3 reaction and definitively assigned it to 3-nitroindole by comparison with chromatograms of nitroindole standards. Mass spectra of aerosolized 3-nitroindole particles were recorded with an aerosol mass spectrometer and directly compared to mass spectra of SOA from smog chamber oxidation of indole by NO_3 in order to help identify peaks unique to nitroindole (m/z 162, 132, and 116). Quantum chemical calculations were done to determine the energetics of hypothesized indole + NO_3 intermediates and products. The combination of these data suggests a mechanism, wherein a hydrogen atom is first abstracted from the N−H bond in indole, followed by isomerization to a carbon-centered radical in the 3-position and followed by addition of NO_2. Alternative mechanisms involving a direct abstraction of a H atom from a C−H bond or a NO_3 addition to the ring are predicted to be energetically unfavorable from large barriers for the initial reaction steps.

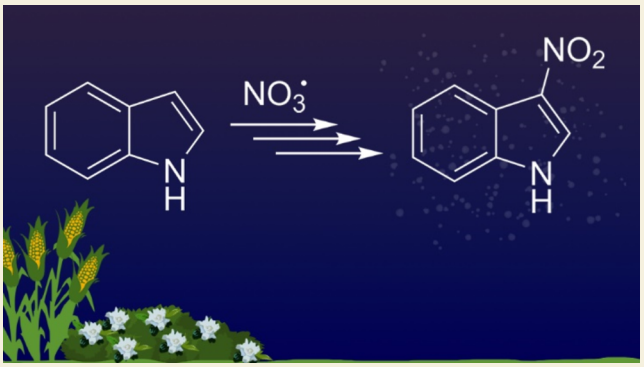

KEYWORDS: *indole, nitrate radical, brown carbon, secondary organic aerosol, nitroaromatic compounds*

INTRODUCTION

The importance of secondary organic aerosol (SOA) in the atmosphere is well established, with many studies highlighting the role of SOA in radiative forcing and cloud formation.[1−10] Various atmospheric oxidants contribute to atmospheric SOA formation from volatile organic compounds (VOCs); however, the nitrate radical (NO_3) is unique in that its strongest contribution occurs during nighttime.[11] Nitrate radical can react with both biogenic and anthropogenic VOCs to produce light-absorbing aerosol.[12−14] Recent studies have examined the formation of SOA from indole, a VOC emitted by plants, revealing strong light absorption by SOA formed by the reaction of indole with NO_3.[15,16]

The nitrate radical reacts with monoterpenes and aromatic compounds by different mechanisms, resulting in nitric acid esters (R-ONO_2) for the former and nitroaromatics (Ar-NO_2) for the latter.[13,17−19] As an aromatic molecule, indole has a higher likelihood of forming aromatic nitro compounds (Ar-NO_2), which are known to be strong chromophores.[20] Accordingly, the dominant chromophore in indole + NO_3 SOA was assigned to be a nitroindole,[15] though definitive assignment of the specific isomer was not possible.

At least a handful of studies have been able to identify the molecular formula of nitroindole ($C_8H_6N_2O_2$) in ambient measurements of organic aerosol,[21−24] with some also finding that it is a major chromophore within the sample.[23,24] Unlike other nitroaromatics, which tend to have higher ambient concentrations in the winter (in conjunction with wood burning), $C_8H_6N_2O_2$ is usually detected in the summer, with potential ties to oil, gas, and diesel emissions.[21,23,25] It remains unconfirmed which nitroindole isomer(s) are present in these samples.

More recent work by Jiang and co-workers proposed that the dominant isomer is 3-nitroindole, though no comparisons were drawn between the SOA and an analytical standard.[16] From their proposed mechanism, it can be assumed that OH and NO_3 act similarly by abstracting a hydrogen from indole, followed by addition of NO_2 to the resulting radical. Although this mechanism is of interest, no studies to date have attempted a computational description of the indole + NO_3 reaction mechanism. The goals of this work are to better constrain the mechanism of indole oxidation and to confirm the identity of the nitroindole isomer formed in the indole +

Received: June 8, 2024
Revised: June 26, 2024
Accepted: June 27, 2024
Published: July 11, 2024

https://doi.org/10.1021/acsphyschemau.4c00044
ACS Phys. Chem Au 2024, 4, 568−574

NO_3 reaction with a combination of experimental and quantum chemical methods.

METHODS

Standards and Aerosol Generation

Reference standards for several nitroindole isomers were prepared in 2-propanol (MilliporeSigma, ACS grade) with mass concentrations around 0.2 mg/mL for UV/vis studies. The nitroindoles investigated were 3-nitroindole (BLD Pharm, solid, 98%), 4-nitroindole, 5-nitroindole, 6-nitroindole, and 7-nitroindole (each from Fisher Scientific, solids, >98%).

Indole + NO_3 SOA was generated in a 5 m^3 smog chamber in batch mode similar to previous work.[15] Nitrate radicals were generated by the simultaneous injection of 200 ppb NO and 500 ppb O_3. Under these conditions, NO is converted into NO_2 by its fast reaction with O_3, and some of the NO_2 is subsequently converted to NO_3 by the residual O_3. Since indole exhibits nearly 10^6 times higher reactivity toward NO_3 than O_3,[26] reactions of indole with NO_3 are favored, even with O_3 being in slight excess of the required stoichiometric ratio. A 40 μL aliquot of a 110 mg/mL solution of indole in methanol was then gently evaporated into a 2 standard liters per minute flow of clean air and passed through a heated inlet into the chamber, yielding an indole mixing ratio around 180 ppb. The temperature and relative humidity (RH) remained relatively constant at 26 °C and 50%, respectively. The SOA was collected after 3 h of reaction by pulling air from the chamber directly through a 0.2 μm PTFE filter (Merck Millipore, 47 mm diameter) for 45 min. The filter sample was extracted in a 1:1 acetonitrile/water mixture, resulting in an SOA solution with an approximate mass concentration of 200 μg/mL.

For experiments with a time-of-flight aerosol mass spectrometer (ToF-AMS, Aerodyne, mass resolving power ~2000), the mass loadings of all reactants were lowered to around 40 ppb indole, 60 ppb NO, and 200 ppb O_3, and the reactions were carried out under dry conditions (<2% RH) to avoid interferences with water in the AMS. Standard 3-nitroindole particles were generated by aerosolizing a 0.10 mg/mL solution of 3-nitroindole in methanol with a constant output atomizer (TSI, model 3076) at ~2 standard liters per minute, sending the flow through two silica gel diffusion driers and a carbon denuder to remove excess methanol, and injecting it into a 130 L Teflon bag.

Spectrophotometry, Chromatography, and Mass Spectrometry Methods

UV/vis absorption spectra for the nitroindole standards dissolved in 2-propanol were recorded over the 200−700 nm range with a Shimadzu UV-2450 spectrophotometer and were converted to molar absorption coefficient spectra using the Beer−Lambert law. Although we did not check for linear dependence, the concentrations were chosen so that the peak in the near-UV had an absorbance of less than 1.

Chromatographic analysis of the SOA (and standards) was carried out with ultra-high-performance liquid chromatography with heated electrospray ionization and high-resolution mass spectrometry (UHPLC-HESI-HRMS). The system consisted of a Vanquish Horizon UHPLC system interfaced to both a photodiode array detector and a Q-Exactive Plus Orbitrap high-resolution mass spectrometer (Thermo Scientific, mass resolving power ~1.4 × 10^5). Additional details of the methods, including eluents, gradients, and instrument settings, can be found in the Supporting information (SI). The formula of the main chromophore in the SOA was verified to be $C_8H_6N_2O_2$, consistent with its previous assignment to a nitroindole isomer.

A scanning mobility particle sizer, consisting of an electrostatic classifier (TSI, model 3080, long DMA) and condensation particle counter (TSI, model 3775), was used to measure size distributions of both the aerosolized 3-nitroindole particles and of the SOA in the smog chamber. Details of the ToF-AMS method and analysis are provided in the Supporting information.

Computational Methods

Electronic structure calculations were done to provide insight into the energetics of a handful of potential indole + NO_3 reaction mechanisms. The Q-Chem 6.0 computational chemistry package was used for the entirety of this work.[27] Density functional theory (DFT) calculations were done with the PBE0 hybrid functional,[28] which has previously been used to estimate bond dissociation energies in other nitroaromatics with absolute errors as low as 1 kcal/mol.[29] For structures more critical to the hypothesized reaction pathway, second-order Møller−Plesset perturbation theory (MP2) was also used to reoptimize structures. The 6-311++G(d,p) basis set was used for all calculations,[30] employing the extra diffuse functions and polarization functions in an attempt to capture the effects of the unpaired electrons in the oxidants (NO_2 and NO_3) and the intermediates.

Harmonic vibrational frequency calculations were done with optimized geometries. The presence of an imaginary frequency was used as an indicator of potential transition state structures. Thermochemistry data were derived from the frequency calculations using the standard formulas implemented in Q-Chem. These data were calculated in standard conditions, and no scaling factors or other corrections were made to the resulting values. References to previous calculations for indole[31] and to experimental measurements in pyrrole (a substructural component of indole) were made to address the accuracy of these theoretical findings.[32]

RESULTS AND DISCUSSION

UV/vis Analysis

The UV/vis absorption spectra of each nitroindole isomer were measured and scaled by their concentrations in 2-propanol to produce the molar absorption coefficients in Figure 1A. The peak positions are summarized in Table S1,

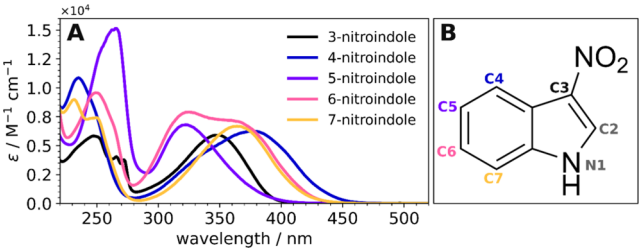

Figure 1. (A) Molar absorption coefficient spectra of the 3-, 4-, 5-, 6-, and 7-nitroindole isomers in 2-propanol. (B) Structure of 3-nitroindole, with numeric labels for the other positions of the indole backbone.

and the spectra are separated into individual plots in Figure S1. The structure of 3-nitroindole and labels for other isomeric positions are provided in Figure 1B. Most isomers exhibit one broadly absorbing peak in the near-UV (300−400 nm) range, although 6-nitroindole has two maxima in this range. The absorption spectrum for 4-nitroindole extends furthest into the visible range. Absorption spectra of 3-nitroindole and 5-nitroindole are largely confined to the near-UV range, with peaks located at 349 and 322 nm, respectively.

Chromatography and PDA-HRMS

The PDA chromatograms for the indole + NO_3 SOA sample reveal a handful of light-absorbing species eluting at various times (Figure S2), in good agreement with previous findings for this type of SOA.[15] The major chromophore eluting at 10.5 min is detectable at m/z 161.0356 ($C_8H_5N_2O_2^-$, −0.3 ppm) in negative ion mode and m/z 163.0500 ($C_8H_7N_2O_2^+$, −1.3 ppm) in positive ion mode. The $C_8H_6N_2O_2$ formula of the

https://doi.org/10.1021/acsphyschemau.4c00044
ACS Phys. Chem Au 2024, 4, 568−574

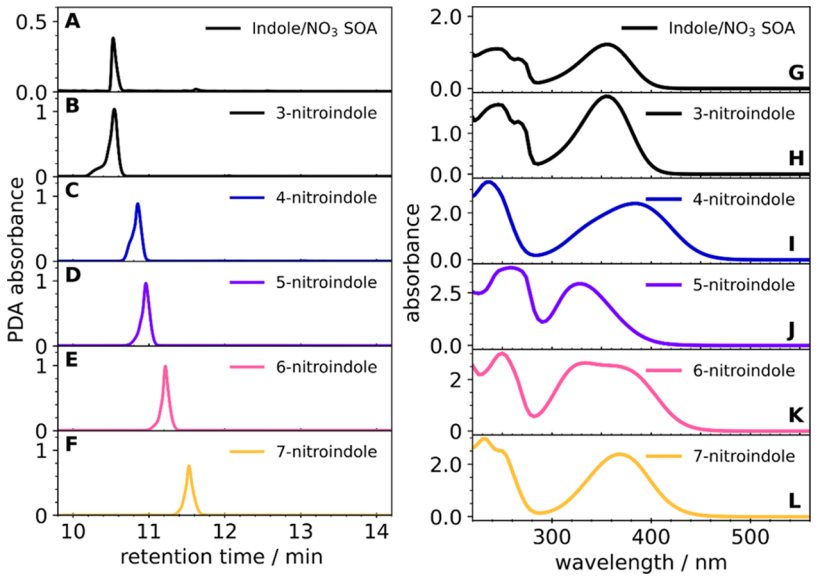

Figure 2. Photodiode array detector chromatograms (integrated from 192−680 nm) for indole + NO_3 SOA and five isomeric nitroindole standards (A−F) and the absorption spectra at the peak of each chromatogram (G−L).

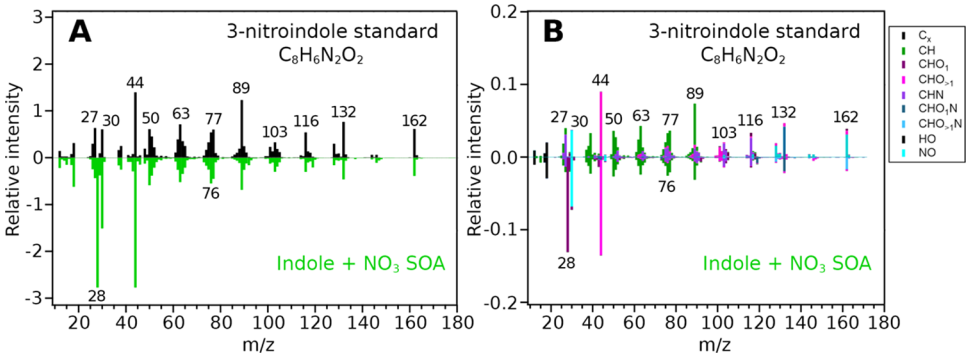

Figure 3. (A) Unit mass resolution and (B) high-resolution ToF-AMS spectra of aerosolized 3-nitroindole particles (top) and indole + NO_3 SOA (bottom).

neutral species is consistent with its previous assignment to a nitroindole isomer. The selected ion chromatograms for these ions (Figure S2) produce a single dominant peak, with other peaks being more than an order of magnitude smaller, suggesting that a single isomer of nitroindole is preferentially formed. This isomer can be unambiguously identified to 3-nitroindole by matching both the PDA retention times (Figure 2A,B) and the PDA UV/vis absorption spectra (Figure 2G,H). It is clear from the combination of these results that the 3-nitroindole isomer is the dominant, if not the only, isomer, which is formed in the indole + NO_3 reaction. Although 2-nitroindole is not commercially available, the exact match of 3-nitroindole toward the SOA chromophore at all three of the 250, 270, and 354 nm peaks is unlikely to be mirrored by 2-nitroindole in view of the large differences between absorption spectra of nitroindole isomers.

Aerosol Mass Spectrometry

Figure 3A shows the unit mass resolution ToF-AMS spectra for indole + NO_3 SOA and the 3-nitroindole standard. There is a striking resemblance between the fragmentation patterns of the 3-nitroindole standard and the SOA. Figure 3B shows the corresponding high-resolution AMS spectra, in which peaks have been assigned up to ~ m/z 120 and the fragment families are shown by color. There is less certainty in the peak assignments above m/z 120 due to the insufficient resolving power of the ToF-AMS instrument, but peaks at m/z 132 and 162 are confidently assigned using the standard as a guide since the molecular ion (M^+) is observed and losses of NO and NO_2 are expected for nitroaromatic compounds.[33] Generation of ToF-AMS spectra for the standard included modifications to the fragmentation tables, which are described in the Supporting information. Briefly, the CO^+ fragment was not fitted for the 3-nitroindole spectra, while default fragmentation tables were used for SOA spectra. NO^+ and NO_2^+ were significant fragments in both nitroindole and SOA spectra and are included in Figure 3 as well.

Proposed assignments to the major fragments observed in the nitroindole standard ToF-AMS spectrum are presented in Table 1. The peak observed at m/z 162 corresponds to the 3-nitroindole radical cation. The peaks at m/z 132 and 116 correspond to the loss of NO and NO_2, respectively, and peaks at lower m/z values are due to more extensive ion fragmentation. Given the strong similarities in ToF-AMS spectra of 3-nitroindole and indole + NO_3 SOA, the dominant ions (m/z 162, 132, and 116) can potentially be used to identify nitroindole in ambient samples. It should be noted that the electron impact ionization (the type of ionization used in ToF-AMS) produces similar ion fragmentation patterns for

https://doi.org/10.1021/acsphyschemau.4c00044
ACS Phys. Chem Au 2024, 4, 568−574

Table 1. Observed Ions with Proposed Formulas and Fragmentation Schemes for Aerosolized 3-Nitroindole Particles Measured with ToF-AMS

m/z	formula	fragmentation scheme
162	$C_8H_6N_2O_2^+$	M^+
132	$C_8H_6NO^+$	$[M\text{-}NO]^+$
116	$C_8H_6N^+$	$[M\text{-}NO_2]^+$
103	$C_7H_5N^+$	$[M\text{-}NO_2\text{-}CH]^+$
89	$C_7H_5^+$	$[M\text{-}NO_2\text{-}CH\text{-}N]^+$

other isomers of nitroindole, so ToF-AMS would detect a collection of all of the isomers.[34]

The overwhelming similarities between the ToF-AMS spectra of the standard and of the SOA are indicative that the indole + NO_3 SOA is predominantly composed of nitroindole. To lend insight into this possibility, the relative ionization efficiency (RIE) of 3-nitroindole was determined in separate experiments described in the Supporting information, following a procedure similar to that of Nault et al.[35] The RIE was found to be $RIE_{3\text{-}NI} = 2.6 \pm 0.6$, which is higher than the default RIE of 1.4 typically used for oxidized organic aerosol. The higher $RIE_{3\text{-}NI}$ indicates a higher sensitivity to 3-nitroindole and its isomers and supports the use of the ions at *m/z* 162, 132, and 116 (particularly when all three are present) to identify the presence of nitroindole isomers in ambient samples. This higher RIE also explains why the AMS spectrum for the indole + NO_3 SOA appears to be dominated by 3-nitroindole, despite other minor species being present in the sample.

Similar AMS spectra were observed by Jiang et al. for indole oxidized by NO_3 with seed particles, in which *m/z* 162 was assigned to $C_{13}H_6^+$ and *m/z* 132 was assigned to $C_5H_8O_4^+$.[16] Based on our results relying on an authentic standard, we assign *m/z* 162 to $C_8H_6N_2O_2^+$ and *m/z* 132 peak to $C_8H_6NO^+$. The use of the 3-nitroindole standard allowed for clear peak assignments for *m/z* 162, 132, and several other prominent nitroindole-related peaks, as shown in Table 1. The combined observations in this work and Jiang et al. make it clear that 3-nitroindole is a dominant component of the indole + NO_3 SOA, and the following sections will provide a mechanistic justification for these observations.

Potential Indole + NO_3 Reaction Mechanisms

The net reaction to convert indole into nitroindole is likely to be described as a reaction of indole, NO_3, and NO_2 to yield nitroindole and HNO_3 in the gas phase. Jiang et al.[16] proposed that the mechanism involves a two-step process, in which the nitrate radical first abstracts a hydrogen from a C−H bond in indole to produce an indole radical and nitric acid (R1). The carbon-centered indole radical can then undergo a recombination reaction with a NO_2 radical to form nitroindole (R2). We should note that the conditions in the current work would allow for the presence of NO_2 through incomplete $NO_2 \rightarrow NO_3$ conversion by O_3.

$$C_8H_7N\ (\text{indole}) + NO_3^\bullet \rightarrow C_8H_6N^\bullet\ (\text{indole radical}) + HNO_3 \quad (R1)$$

$$C_8H_6N^\bullet + NO_2^\bullet \rightarrow C_8H_6N_2O_2\ (\text{nitroindole}) \quad (R2)$$

The hydrogen abstraction reaction R1 should proceed at the position of the weakest bond in indole. Jiang et al.[16] assumed that the H atom in C3 is the one that is being abstracted, which is a reasonable guess. To our knowledge, no measurements of bond dissociation energies (BDEs) have been reported for indole, however, theoretical calculations have estimated the BDE of each of its C−H bonds and the N−H bond. These calculations, done with B3LYP/6-31G(d), suggest that the C−H bonds on the benzene ring of indole are weaker (111.1−111.5 kcal/mol) compared to the pyrrole ring (117.5 kcal/mol at C2, 118.0 kcal/mol at C3).[31] Studies of the reaction between NO_3 and benzene have shown that the hydrogens in benzene are resistant toward hydrogen abstraction,[36,37] and this characteristic likely translates to indole as well. It is also worth noting that the N−H bond is predicted to be much weaker (86.9 kcal/mol),[31] which could indicate that hydrogen abstraction could occur from the N−H bond, as opposed to a C−H bond.

A similar mechanism proposed by Mayorga et al. proposed that hydrogen abstraction occurs from the N−H bond in pyrrole.[38] Importantly, the resulting nitrogen-centered radical is stabilized by resonance, which shifts the free electron to form a carbon-centered radical at C3. A similar process could reasonably occur on the pyrrole ring of indole, as is shown in Figure 4. Hydrogen abstraction from the nitrogen results in a pair of resonance-stabilized intermediates (IM1 and IM2). The resonance does not readily extend to the more stable benzene ring in indole, leading to the dominant formation of 3-nitroindole in indole oxidation by NO_3 and potentially OH/NO_2. The most uncertain part of this mechanism is the last step, which is regarded to be a 1,3 hydrogen shift in pyrrole.[38] Such a process is also possible in indole.

We also considered an alternative mechanism, in which the NO_3 attaches to the closed-shell indole, followed by addition of NO_2 and elimination of HNO_3. A computational study by Li et al.[39] of the reaction of indole with acetonitrile (CH_2CN) and trifluoromethyl (CF_3) radicals found that these radicals preferentially attach to C2. It should be noted that their study was approaching this problem from the perspective of synthetic organic chemistry, with an emphasis on these reactions as they might occur in a solvent. For that reason, radical reactions with the N−H bond were perhaps ignored in that work. While the insights regarding the energetics of radical addition brought from that study are useful (they did provide results for the gas phase), the subsequent reaction steps (namely, deprotonation) outlined in that work are likely to be less applicable to the gas-phase setting of this indole + NO_3 organic aerosol formation.

The following discussion will show that the mechanism in Figure 4 is energetically favored, and mechanisms involving the

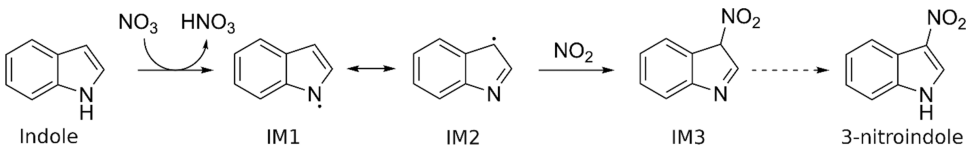

Figure 4. Proposed hydrogen abstraction mechanism for the formation of 3-nitroindole from the reaction of indole and NO_3.

https://doi.org/10.1021/acsphyschemau.4c00044
ACS Phys. Chem Au 2024, 4, 568−574

abstraction of hydrogen from a C−H bond or NO_3 attachment are less favorable. More results around the NO_3 attachment mechanism have been placed in the Supporting information.

Computational Results for Hydrogen Abstraction

The thermochemistry data resulting from the electronic structure calculations of the products of hydrogen abstraction at each position are provided in Table 2. DFT at the PBE0/6-311++G(d,p) level was used for all abstractable hydrogen atoms since PBE0 was shown to produce reaction and activation energies within 2.4 kcal/mol (root-mean-square error) for hydrogen abstraction reactions in polycyclic aromatic hydrocarbons.[40] We used the higher level MP2/6-311++G(d,p) only for abstraction at N1, C2, and C3 to minimize computational expense. The PBE0/6-311++G(d,p) calculations were sufficiently accurate, as the estimated BDEs were similar to those calculated in previous studies and comparable to those measured in pyrrole.[31] The initial step (reaction R1) is energetically uphill for H abstraction from any of the C−H bonds and slightly more so for the C−H bonds in the 2 and 3 positions (C2 and C3). Importantly, only the abstraction from the N−H bond is predicted to be exergonic.

Table 2. Thermochemistry Data at the PBE0/6-311++G(d,p) and [MP2/6-311++G(d,p)] Levels for Hydrogen Abstraction Reaction R1

reaction site	$\Delta(E + ZPE)$ (kcal/mol)	ΔH (kcal/mol)	ΔG (kcal/mol)
C2	14.8 [18.9]	16.8 [26.4]	16.5 [26.5]
C3	15.5 [21.5]	17.7 [29.5]	17.7 [29.9]
C4	8.5	10.6	10.5
C5	8.4	10.4	10.3
C6	8.4	10.4	10.4
C7	8.8	11.0	10.9
N1	−10.6 [−6.1]	−9.3 [−2.8]	−9.3 [−2.5]

A stepwise presentation of the reaction energetics for the indole + NO_3 + NO_2 pathway for hydrogen abstraction from N1 is presented in Figure 5. All energy values correspond to the minimized structures, with exception to IM1, which was approximated by simply removing the N1 hydrogen from the minimized indole structure. Optimization of IM1 resulted in IM2, consistent with the lower energy of the latter. For the hydrogen abstraction reaction, intermediates IM1 and IM2 result from abstraction from N1 and are both energetically favorable, with the carbon-centered radical form being the most stable. The spin density is shown to highlight the shifting of the unpaired electron to be predominantly around C3 in the IM2 structure.

Reaction R2, being a radical recombination reaction, should happen efficiently and potentially be barrierless.[41] The former is supported by the overall reaction being highly exergonic. While the remaining steps between IM3 and 3-nitroindole are uncertain, there is evidence that the yield for the IM3 → 3-nitroindole process is almost 100% due to the striking lack of other isomers in the selected ion chromatograms (Figure S2).

Given that the mechanism should be able to describe both OH- and NO_3-initiated reactions, the conversion from IM3 to 3-nitroindole is likely to proceed via an internal hydrogen shift. No attempt was made to model this process in this work. The simplest explanation would be that the excess energy after recombination would result in having sufficient energy for the internal hydrogen shift process, for example, by tunneling. More complex reactions with other molecules that first remove the hydrogen from C3 in IM3 and then reinstall it back to the N1 nitrogen are also possible. Given the energetic benefit of switching from IM3 to 3-nitroindole, the hydrogen shift is the likely option, resulting in dominant yields of 3-nitroindole.

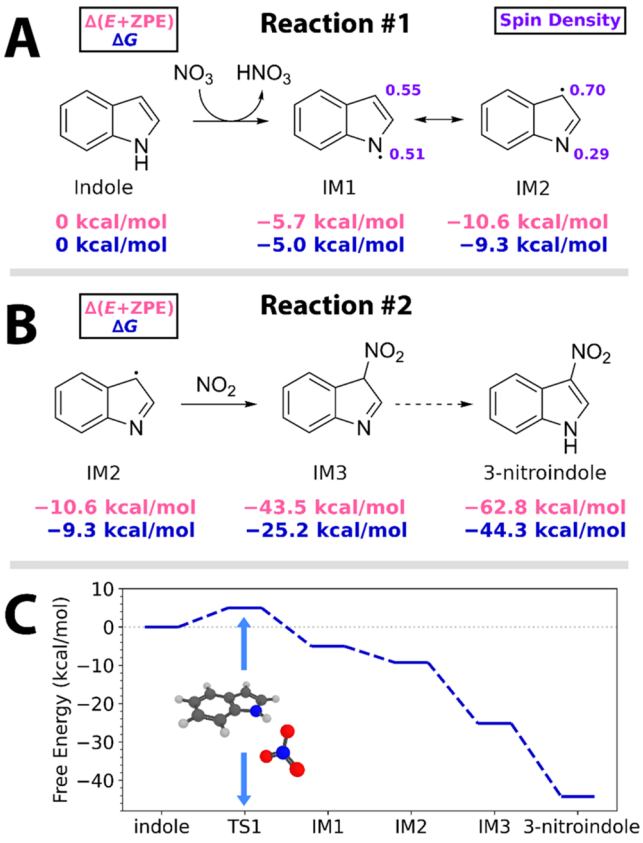

Figure 5. Thermochemical results at the PBE0/6-311++G(d,p) level for the hydrogen abstraction mechanism initiated by removal of the hydrogen at the N position (N1). $\Delta(E + ZPE)$ values are provided in pink, and ΔG values are provided in blue, with reference to the reactants (including the oxidant) in each reaction.

CONCLUSIONS

This work has provided strong evidence that 3-nitroindole is the major molecular component of indole + NO_3 secondary organic aerosol. The identification was confirmed by matching the retention time in chromatography, the shape of the absorption spectrum in UV/vis spectroscopy, and the accurate mass-to-charge ratio in mass spectrometry. Furthermore, we were able to provide mechanistic justification for the dominant formation of 3-nitroindole with the aid of electronic structure calculations. The most likely mechanism appears to be initiated by NO_3 abstracting the hydrogen from the indole's N−H bond. Through resonance, the free electron density is shifted to the carbon in the 3-position of indole, priming the indole radical for a recombination reaction with NO_2, producing 3-nitroindole. We were able to rule out alternative mechanisms, in which NO_3 either abstracts a hydrogen atom directly from a C−H bond or is added to indole instead of abstracting a hydrogen atom.

The ToF-AMS mass spectra were also remarkably similar between the indole + NO_3 SOA and 3-nitroindole standard, with the parent ion (m/z 162) present in both the SOA and the standard. Various fragmentation peaks were also present and shared similarities to electron ionization mass spectra of

https://doi.org/10.1021/acsphyschemau.4c00044
ACS Phys. Chem Au 2024, 4, 568−574

nitroindoles in the literature. It may be worth extending the m/z range of ToF-AMS analysis to larger m/z, namely, looking for the pattern of 116, 132, and 162, when there is potential for indole oxidation products to be present, such as ambient measurements near animal husbandry facilities or during times of significant plant blooming.

■ ASSOCIATED CONTENT

Supporting Information

The Supporting Information is available free of charge at https://pubs.acs.org/doi/10.1021/acsphyschemau.4c00044.

Description of the effect of solvent on absorption spectra of nitroindole isomers; further details of the UHPLC methods; description of the unfavorable NO_3 attachment mechanism to indole; details of the ToF-AMS measurements and analysis, generation of AMS spectra, and determination of the relative ionization efficiency of 3-nitroindole (PDF)

Tabulated molar absorption coefficients of nitroindole isomers from Figure 1 (TXT)

■ AUTHOR INFORMATION

Corresponding Author

Sergey A. Nizkorodov − *Department of Chemistry, University of California, Irvine, California 92697, United States;* orcid.org/0000-0003-0891-0052; Email: nizkorod@uci.edu

Authors

Avery B. Dalton − *Department of Chemistry, University of California, Irvine, California 92697, United States;* orcid.org/0000-0002-6923-9090

Lisa M. Wingen − *Department of Chemistry, University of California, Irvine, California 92697, United States;* orcid.org/0000-0001-5847-9913

Complete contact information is available at: https://pubs.acs.org/10.1021/acsphyschemau.4c00044

Notes

The authors declare no competing financial interest.

■ ACKNOWLEDGMENTS

This work was supported by the US National Science Foundation grant AGS-2334731. The high-resolution mass spectrometer instrument used in this work was purchased with the US National Science Foundation grant CHE-1920242.

■ REFERENCES

(1) Maria, S. F.; Russell, L. M.; Gilles, M. K.; Myneni, S. C. B. Organic Aerosol Growth Mechanisms and Their Climate-Forcing Implications. *Science* **2004**, *306* (5703), 1921−1924.

(2) Hoyle, C. R.; Myhre, G.; Berntsen, T. K.; Isaksen, I. S. A. Anthropogenic Influence on SOA and the Resulting Radiative Forcing. *Atmos. Chem. Phys.* **2009**, *9* (8), 2715−2728.

(3) Spracklen, D. V.; Jimenez, J. L.; Carslaw, K. S.; Worsnop, D. R.; Evans, M. J.; Mann, G. W.; Zhang, Q.; Canagaratna, M. R.; Allan, J.; Coe, H.; McFiggans, G.; Rap, A.; Forster, P. Aerosol Mass Spectrometer Constraint on the Global Secondary Organic Aerosol Budget. *Atmos. Chem. Phys.* **2011**, *11* (23), 12109−12136.

(4) Li, K.; Li, J.; Liggio, J.; Wang, W.; Ge, M.; Liu, Q.; Guo, Y.; Tong, S.; Li, J.; Peng, C.; Jing, B.; Wang, D.; Fu, P. Enhanced Light Scattering of Secondary Organic Aerosols by Multiphase Reactions. *Environ. Sci. Technol.* **2017**, *51* (3), 1285−1292.

(5) Aiona, P. K.; Luek, J. L.; Timko, S. A.; Powers, L. C.; Gonsior, M.; Nizkorodov, S. A. Effect of Photolysis on Absorption and Fluorescence Spectra of Light-Absorbing Secondary Organic Aerosols. *ACS Earth Space Chem.* **2018**, *2* (3), 235−245.

(6) Zahardis, J.; Petrucci, G. A. The Oleic Acid-Ozone Heterogeneous Reaction System: Products, Kinetics, Secondary Chemistry, and Atmospheric Implications of a Model System − a Review. *Atmos. Chem. Phys.* **2007**, *7* (5), 1237−1274.

(7) Murray, B. J. Inhibition of Ice Crystallisation in Highly Viscous Aqueous Organic Acid Droplets. *Atmos. Chem. Phys.* **2008**, *8* (17), 5423−5433.

(8) Koop, T.; Bookhold, J.; Shiraiwa, M.; Pöschl, U. Glass Transition and Phase State of Organic Compounds: Dependency on Molecular Properties and Implications for Secondary Organic Aerosols in the Atmosphere. *Phys. Chem. Chem. Phys.* **2011**, *13* (43), 19238−19255.

(9) Berkemeier, T.; Shiraiwa, M.; Pöschl, U.; Koop, T. Competition between Water Uptake and Ice Nucleation by Glassy Organic Aerosol Particles. *Atmos. Chem. Phys.* **2014**, *14* (22), 12513−12531.

(10) Schill, G. P.; De Haan, D. O.; Tolbert, M. A. Heterogeneous Ice Nucleation on Simulated Secondary Organic Aerosol. *Environ. Sci. Technol.* **2014**, *48* (3), 1675−1682.

(11) Edwards, P. M.; Aikin, K. C.; Dube, W. P.; Fry, J. L.; Gilman, J. B.; de Gouw, J. A.; Graus, M. G.; Hanisco, T. F.; Holloway, J.; Hübler, G.; Kaiser, J.; Keutsch, F. N.; Lerner, B. M.; Neuman, J. A.; Parrish, D. D.; Peischl, J.; Pollack, I. B.; Ravishankara, A. R.; Roberts, J. M.; Ryerson, T. B.; Trainer, M.; Veres, P. R.; Wolfe, G. M.; Warneke, C.; Brown, S. S. Transition from High- to Low-NOx Control of Night-Time Oxidation in the Southeastern US. *Nat. Geosci.* **2017**, *10* (7), 490−495.

(12) Joo, T.; Rivera-Rios, J. C.; Takeuchi, M.; Alvarado, M. J.; Ng, N. L. Secondary Organic Aerosol Formation from Reaction of 3-Methylfuran with Nitrate Radicals. *ACS Earth Space Chem.* **2019**, *3* (6), 922−934.

(13) He, Q.; Tomaz, S.; Li, C.; Zhu, M.; Meidan, D.; Riva, M.; Laskin, A.; Brown, S. S.; George, C.; Wang, X.; Rudich, Y. Optical Properties of Secondary Organic Aerosol Produced by Nitrate Radical Oxidation of Biogenic Volatile Organic Compounds. *Environ. Sci. Technol.* **2021**, *55* (5), 2878−2889.

(14) Mayorga, R. J.; Zhao, Z.; Zhang, H. Formation of Secondary Organic Aerosol from Nitrate Radical Oxidation of Phenolic VOCs: Implications for Nitration Mechanisms and Brown Carbon Formation. *Atmos. Environ.* **2021**, *244*, No. 117910.

(15) Baboomian, V. J.; He, Q.; Montoya-Aguilera, J.; Ali, N.; Fleming, L. T.; Lin, P.; Laskin, A.; Laskin, J.; Rudich, Y.; Nizkorodov, S. A. Light Absorption and Scattering Properties of Indole Secondary Organic Aerosol Prepared under Various Oxidant and Relative Humidity Conditions. *Aerosol Sci. Technol.* **2023**, *57* (6), 532−545.

(16) Jiang, F.; Siemens, K.; Linke, C.; Li, Y.; Gong, Y.; Leisner, T.; Laskin, A.; Saathoff, H. Molecular Analysis of Secondary Organic Aerosol and Brown Carbon from the Oxidation of Indole. *Atmos. Chem. Phys.* **2024**, *24* (4), 2639−2649.

(17) Ng, N. L.; Kwan, A. J.; Surratt, J. D.; Chan, A. W. H.; Chhabra, P. S.; Sorooshian, A.; Pye, H. O. T.; Crounse, J. D.; Wennberg, P. O.; Flagan, R. C.; Seinfeld, J. H. Secondary Organic Aerosol (SOA) Formation from Reaction of Isoprene with Nitrate Radicals (NO_3). *Atmos. Chem. Phys.* **2008**, *8* (14), 4117−4140.

(18) Perraud, V.; Bruns, E. A.; Ezell, M. J.; Johnson, S. N.; Yu, Y.; Alexander, M. L.; Zelenyuk, A.; Imre, D.; Chang, W. L.; Dabdub, D.; Pankow, J. F.; Finlayson-Pitts, B. J. Nonequilibrium Atmospheric Secondary Organic Aerosol Formation and Growth. *Proc. Natl. Acad. Sci. U.S.A.* **2012**, *109* (8), 2836−2841.

(19) Fry, J. L.; Draper, D. C.; Barsanti, K. C.; Smith, J. N.; Ortega, J.; Winkler, P. M.; Lawler, M. J.; Brown, S. S.; Edwards, P. M.; Cohen, R. C.; Lee, L. Secondary Organic Aerosol Formation and Organic Nitrate Yield from NO_3 Oxidation of Biogenic Hydrocarbons. *Environ. Sci. Technol.* **2014**, *48* (20), 11944−11953.

(20) Yan, J.; Wang, X.; Gong, P.; Wang, C. Nitrated Polycyclic Aromatic Compounds in the Atmospheric Environment: A Review. *Crit. Rev. Environ. Sci. Technol.* **2021**, *51* (11), 1159−1185, DOI: 10.1080/10643389.2020.1748486.
(21) Boris, A. J.; Napolitano, D. C.; Herckes, P.; Clements, A. L.; Collett, J. L., Jr Fogs and Air Quality on the Southern California Coast. *Aerosol Air Qual. Res.* **2018**, *18* (1), 224−239, DOI: 10.4209/aaqr.2016.11.0522.
(22) Zuth, C.; Vogel, A. L.; Ockenfeld, S.; Huesmann, R.; Hoffmann, T. Ultrahigh-Resolution Mass Spectrometry in Real Time: Atmospheric Pressure Chemical Ionization Orbitrap Mass Spectrometry of Atmospheric Organic Aerosol. *Anal. Chem.* **2018**, *90* (15), 8816−8823.
(23) Yan, C.; Zheng, M.; Desyaterik, Y.; Sullivan, A. P.; Wu, Y.; Collett, J. L., Jr. Molecular Characterization of Water-Soluble Brown Carbon Chromophores in Beijing, China. *J. Geophys. Res.: Atmos.* **2020**, *125* (15), No. e2019JD032018.
(24) Li, H.; Qin, X.; Chen, J.; Wang, G.; Liu, C.; Lu, D.; Zheng, H.; Song, X.; Gao, Q.; Xu, J.; Zhu, Y.; Liu, J.; Wang, X.; Deng, C.; Huang, K. Continuous Measurement and Molecular Compositions of Atmospheric Water-Soluble Brown Carbon in the Nearshore Marine Boundary Layer of Northern China: Secondary Formation and Influencing Factors. *J. Geophys. Res.: Atmos.* **2023**, *128* (12), No. e2023JD038565.
(25) Bayona, J. M.; Markides, K. E.; Lee, M. L. Characterization of Polar Polycyclic Aromatic Compounds in a Heavy-Duty Diesel Exhaust Particulate by Capillary Column Gas Chromatography and High-Resolution Mass Spectrometry. *Environ. Sci. Technol.* **1988**, *22* (12), 1440−1447.
(26) Atkinson, R.; Tuazon, E. C.; Arey, J.; Aschmann, S. M. Atmospheric and Indoor Chemistry of Gas-Phase Indole, Quinoline, and Isoquinoline. *Atmos. Environ.* **1995**, *29* (23), 3423−3432.
(27) Epifanovsky, E.; Gilbert, A. T. B.; Feng, X.; Lee, J.; Mao, Y.; Mardirossian, N.; Pokhilko, P.; White, A. F.; Coons, M. P.; Dempwolff, A. L.; Gan, Z.; Hait, D.; Horn, P. R.; Jacobson, L. D.; Kaliman, I.; Kussmann, J.; Lange, A. W.; Lao, K. U.; Levine, D. S.; Liu, J.; McKenzie, S. C.; Morrison, A. F.; Nanda, K. D.; Plasser, F.; Rehn, D. R.; Vidal, M. L.; You, Z.-Q.; Zhu, Y.; Alam, B.; Albrecht, B. J.; Aldossary, A.; Alguire, E.; Andersen, J. H.; Athavale, V.; Barton, D.; Begam, K.; Behn, A.; Bellonzi, N.; Bernard, Y. A.; Berquist, E. J.; Burton, H. G. A.; Carreras, A.; Carter-Fenk, K.; Chakraborty, R.; Chien, A. D.; Closser, K. D.; Cofer-Shabica, V.; Dasgupta, S.; de Wergifosse, M.; Deng, J.; Diedenhofen, M.; Do, H.; Ehlert, S.; Fang, P.-T.; Fatehi, S.; Feng, Q.; Friedhoff, T.; Gayvert, J.; Ge, Q.; Gidofalvi, G.; Goldey, M.; Gomes, J.; González-Espinoza, C. E.; Gulania, S.; Gunina, A. O.; Hanson-Heine, M. W. D.; Harbach, P. H. P.; Hauser, A.; Herbst, M. F.; Hernández Vera, M.; Hodecker, M.; Holden, Z. C.; Houck, S.; Huang, X.; Hui, K.; Huynh, B. C.; Ivanov, M.; Jász, Á.; Ji, H.; Jiang, H.; Kaduk, B.; Kähler, S.; Khistyaev, K.; Kim, J.; Kis, G.; Klunzinger, P.; Koczor-Benda, Z.; Koh, J. H.; Kosenkov, D.; Koulias, L.; Kowalczyk, T.; Krauter, C. M.; Kue, K.; Kunitsa, A.; Kus, T.; Ladjánszki, I.; Landau, A.; Lawler, K. V.; Lefrancois, D.; Lehtola, S.; Li, R. R.; Li, Y.-P.; Liang, J.; Liebenthal, M.; Lin, H.-H.; Lin, Y.-S.; Liu, F.; Liu, K.-Y.; Loipersberger, M.; Luenser, A.; Manjanath, A.; Manohar, P.; Mansoor, E.; Manzer, S. F.; Mao, S.-P.; Marenich, A. V.; Markovich, T.; Mason, S.; Maurer, S. A.; McLaughlin, P. F.; Menger, M. F. S. J.; Mewes, J.-M.; Mewes, S. A.; Morgante, P.; Mullinax, J. W.; Oosterbaan, K. J.; Paran, G.; Paul, A. C.; Paul, S. K.; Pavošević, F.; Pei, Z.; Prager, S.; Proynov, E. I.; Rák, Á.; Ramos-Cordoba, E.; Rana, B.; Rask, A. E.; Rettig, A.; Richard, R. M.; Rob, F.; Rossomme, E.; Scheele, T.; Scheurer, M.; Schneider, M.; Sergueev, N.; Sharada, S. M.; Skomorowski, W.; Small, D. W.; Stein, C. J.; Su, Y.-C.; Sundstrom, E. J.; Tao, Z.; Thirman, J.; Tornai, G. J.; Tsuchimochi, T.; Tubman, N. M.; Veccham, S. P.; Vydrov, O.; Wenzel, J.; Witte, J.; Yamada, A.; Yao, K.; Yeganeh, S.; Yost, S. R.; Zech, A.; Zhang, I. Y.; Zhang, X.; Zhang, Y.; Zuev, D.; Aspuru-Guzik, A.; Bell, A. T.; Besley, N. A.; Bravaya, K. B.; Brooks, B. R.; Casanova, D.; Chai, J.-D.; Coriani, S.; Cramer, C. J.; Cserey, G.; DePrince, A. E., III; DiStasio, R. A., Jr.; Dreuw, A.; Dunietz, B. D.; Furlani, T. R.; Goddard, W. A., III; Hammes-Schiffer, S.; Head-Gordon, T.; Hehre, W. J.; Hsu, C.-P.; Jagau, T.-C.; Jung, Y.; Klamt, A.; Kong, J.; Lambrecht, D. S.; Liang, W.; Mayhall, N. J.; McCurdy, C. W.; Neaton, J. B.; Ochsenfeld, C.; Parkhill, J. A.; Peverati, R.; Rassolov, V. A.; Shao, Y.; Slipchenko, L. V.; Stauch, T.; Steele, R. P.; Subotnik, J. E.; Thom, A. J. W.; Tkatchenko, A.; Truhlar, D. G.; Van Voorhis, T.; Wesolowski, T. A.; Whaley, K. B.; Woodcock, H. L., III; Zimmerman, P. M.; Faraji, S.; Gill, P. M. W.; Head-Gordon, M.; Herbert, J. M.; Krylov, A. I. Software for the Frontiers of Quantum Chemistry: An Overview of Developments in the Q-Chem 5 Package. *J. Chem. Phys.* **2021**, *155* (8), No. 084801.
(28) Adamo, C.; Barone, V. Toward Reliable Density Functional Methods without Adjustable Parameters: The PBE0 Model. *J. Chem. Phys.* **1999**, *110* (13), 6158−6170.
(29) Su, X. F.; Huang, W.; Wu, H. Y. Assessment of PBE0 Calculation of C-NO_2 Bond Dissociation Energies for Nitroaromatic System. *Adv. Mater. Res.* **2014**, *915*−*916*, 675−678.
(30) Krishnan, R.; Binkley, J. S.; Seeger, R.; Pople, J. A. Self-consistent Molecular Orbital Methods. XX. A Basis Set for Correlated Wave Functions. *J. Chem. Phys.* **1980**, *72* (1), 650−654.
(31) Barckholtz, C.; Barckholtz, T. A.; Hadad, C. M. C−H and N−H Bond Dissociation Energies of Small Aromatic Hydrocarbons. *J. Am. Chem. Soc.* **1999**, *121* (3), 491−500.
(32) Blank, D. A.; North, S. W.; Lee, Y. T. The Ultraviolet Photodissociation Dynamics of Pyrrole. *Chem. Phys.* **1994**, *187* (1), 35−47.
(33) Ramdahl, T.; Zielinska, B.; Arey, J.; Kondrat, R. W. The Electron Impact Mass Spectra of Di- and Trinitrofluoranthenes. *Biomed. Environ. Mass Spectrom.* **1988**, *17* (1), 55−62.
(34) Wallace, W. E. Mass Spectra *NIST Chemistry WebBook, NIST Standard Reference Database Number 69*, National Institute of Standards and Technology.
(35) Nault, B. A.; Croteau, P.; Jayne, J.; Williams, A.; Williams, L.; Worsnop, D.; Katz, E. F.; DeCarlo, P. F.; Canagaratna, M. Laboratory Evaluation of Organic Aerosol Relative Ionization Efficiencies in the Aerodyne Aerosol Mass Spectrometer and Aerosol Chemical Speciation Monitor. *Aerosol Sci. Technol.* **2023**, *57* (10), 981−997.
(36) Atkinson, R. Kinetics and Mechanisms of the Gas-Phase Reactions of the NO_3 Radical with Organic Compounds. *J. Phys. Chem. Ref. Data* **1991**, *20* (3), 459−507.
(37) Ren, Y.; Zhou, L.; Mellouki, A.; Daële, V.; Idir, M.; Brown, S. S.; Ruscic, B.; Paton, R. S.; McGillen, M. R.; Ravishankara, A. R. Reactions of NO_3 with Aromatic Aldehydes: Gas-Phase Kinetics and Insights into the Mechanism of the Reaction. *Atmos. Chem. Phys.* **2021**, *21* (17), 13537−13551.
(38) Mayorga, R.; Chen, K.; Raeofy, N.; Woods, M.; Lum, M.; Zhao, Z.; Zhang, W.; Bahreini, R.; Lin, Y.-H.; Zhang, H. Chemical Structure Regulates the Formation of Secondary Organic Aerosol and Brown Carbon in Nitrate Radical Oxidation of Pyrroles and Methylpyrroles. *Environ. Sci. Technol.* **2022**, *56* (12), 7761−7770.
(39) Li, Y.; Vaz, R. J.; Olson, S. H.; Munson, M.; Paras, N. A.; Conrad, J. Selectivity in the Addition of Electron-Deficient Radicals to the C2 Position of Indoles. *Eur. J. Org. Chem.* **2020**, *2020* (36), 5828−5832.
(40) Carissan, Y.; Klopper, W. Hydrogen Abstraction from Biphenyl, Acenaphthylene, Naphthalene and Phenanthrene by Atomic Hydrogen and Methyl Radical: DFT and G3(MP2)-RAD Data. *J. Mol. Struct.: THEOCHEM* **2010**, *940* (1), 115−118, DOI: 10.1016/j.theochem.2009.10.017.
(41) Piletic, I. R.; Edney, E. O.; Bartolotti, L. J. Barrierless Reactions with Loose Transition States Govern the Yields and Lifetimes of Organic Nitrates Derived from Isoprene. *J. Phys. Chem. A* **2017**, *121* (43), 8306−8321.

https://doi.org/10.1021/acsphyschemau.4c00044
ACS Phys. Chem Au 2024, 4, 568−574